

Probing the electronic structures of low oxidation-state uranium fluoride molecules UF_x (x = 24)

Wei-Li Li, Han-Shi Hu, Tian Jian, Gary V. Lopez, Jing Su, Jun Li, and Lai-Sheng Wang

Citation: *The Journal of Chemical Physics* **139**, 244303 (2013); doi: 10.1063/1.4851475

View online: <http://dx.doi.org/10.1063/1.4851475>

View Table of Contents: <http://scitation.aip.org/content/aip/journal/jcp/139/24?ver=pdfcov>

Published by the [AIP Publishing](#)

Articles you may be interested in

Resonant photoelectron spectroscopy of Au₂ via a Feshbach state using high-resolution photoelectron imaging
J. Chem. Phys. **139**, 194306 (2013); 10.1063/1.4830408

Note: Photoelectron spectroscopy of cold UF₅

J. Chem. Phys. **137**, 116101 (2012); 10.1063/1.4753421

Probing the structures and chemical bonding of boron-boronyl clusters using photoelectron spectroscopy and computational chemistry: B₄(BO)_n (n = 1–3)

J. Chem. Phys. **137**, 044307 (2012); 10.1063/1.4737863

Photoelectron spectroscopy and theoretical studies of UF₅ and UF₆

J. Chem. Phys. **136**, 194304 (2012); 10.1063/1.4716182

Probing the structural and electronic properties of Ag_nH (n = 1–3) using photoelectron imaging and theoretical calculations

J. Chem. Phys. **136**, 184312 (2012); 10.1063/1.4713938



Re-register for Table of Content Alerts

Create a profile.



Sign up today!



Probing the electronic structures of low oxidation-state uranium fluoride molecules UF_x^- ($x = 2-4$)

Wei-Li Li,¹ Han-Shi Hu,^{2,3} Tian Jian,¹ Gary V. Lopez,¹ Jing Su,² Jun Li,^{2,3,a)}
 and Lai-Sheng Wang^{1,b)}

¹Department of Chemistry, Brown University, Providence, Rhode Island 02912, USA

²Department of Chemistry & Key Laboratory of Organic Optoelectronics and Molecular Engineering of Ministry of Education, Tsinghua University, Beijing 100084, China

³William R. Wiley Environmental Molecular Sciences Laboratory, Pacific Northwest National Laboratory, Richland, Washington 99352, USA

(Received 10 October 2013; accepted 4 December 2013; published online 26 December 2013)

We report the experimental observation of gaseous UF_x^- ($x = 2-4$) anions, which are investigated using photoelectron spectroscopy and relativistic quantum chemistry. Vibrationally resolved photoelectron spectra are obtained for all three species and the electron affinities of UF_x ($x = 2-4$) are measured to be 1.16(3), 1.09(3), and 1.58(3) eV, respectively. Significant multi-electron transitions are observed in the photoelectron spectra of $U(5f^37s^2)F_2^-$, as a result of strong electron correlation effects of the two $7s$ electrons. The U–F symmetric stretching vibrational modes are resolved for the ground states of all UF_x ($x = 2-4$) neutrals. Theoretical calculations are performed to qualitatively understand the photoelectron spectra. The entire UF_x^- and UF_x ($x = 1-6$) series are considered theoretically to examine the trends of U–F bonding and the electron affinities as a function of fluorine coordination. The increased U–F bond lengths and decreased bond orders from UF_2^- to UF_4^- indicate that the U–F bonding becomes weaker as the oxidation state of U increases from I to III.
 © 2013 AIP Publishing LLC. [<http://dx.doi.org/10.1063/1.4851475>]

I. INTRODUCTION

Actinide chemistry has attracted significant recent attention because of the importance of nuclear energy and the issues related to the disposal of nuclear wastes. Understanding the electronic structures and chemical bonding of uranium compounds is important for developing efficient extraction agents for nuclear waste management and advanced nuclear fuel cycle.¹ The most common and most important uranium fluoride is uranium hexafluoride (UF_6), which is used in the nuclear industry for isotope separation to produce ^{235}U -enriched nuclear fuels. The UF_6 molecule in the gas phase has been extensively studied both experimentally and theoretically.²⁻³¹ It is a perfect octahedral molecule (O_h symmetry) with a U–F bond length of $1.996 \pm 0.008 \text{ \AA}$,² in which U is in its most stable oxidation state of VI. UF_5 is a photolysis product of UF_6 and can be produced by reactions of uranium with fluorine.⁶ The UF_5 molecule, which has C_{4v} symmetry, has also been well characterized.^{5-7,31-35} Uranium tetrafluoride (UF_4) is a stable compound, in which U has an oxidation of U^{4+} ($5f^2$). The UF_4 molecule in the gas phase has T_d symmetry with a bond length of $2.056 \pm 0.001 \text{ \AA}$.^{36,37} However, there have been suggestions that UF_4 may have a distorted tetrahedral structure due to the Jahn-Teller effect.³⁸⁻⁴¹ More recent infrared spectroscopy data seem to support the T_d symmetry in the gas phase.^{37,42}

Although there have been extensive investigations on the UF_x ($x = 4-6$) molecules, much less is known about the

lower oxidation-state UF_x species, primarily because these are all transient species and are expected to be highly reactive. UF_x^+ ($x = 1-4$) cations were observed by mass spectrometry.³² UF_x ($x = 1-3$) species were proposed to exist in noble gas matrix,³³ but the absorption spectra attributed to UF and UF_2 were later reassigned to HF dimer and trimer, respectively.^{42,43} Only very recently, a spectroscopic and theoretical study is reported on the diatomic UF and UF^+ species.⁴³ Even though there have been a number of theoretical investigations on the geometries and vibration frequencies of UF_x ($x = 1-6$) systematically,⁴⁴⁻⁴⁸ there is little experimental information available for low oxidation-state uranium fluoride species. The low oxidation state UF_x species with unpaired $5f$ or $7s$ electrons are expected to exhibit more complicated electronic structures and possess rich spectroscopic information, which will provide better systems to compare with theoretical calculations and verify new computational methods. Our recent investigation on UO_2^- , which has a $(7s)^2(5f^1)$ electron configuration, illustrates an example that gives extremely rich photoelectron spectra due to strong electron correlation effects.⁴⁹ Accurate calculations involving both the initial and final states, with inclusion of electron correlation and spin-orbit coupling effects, are needed to interpret the observed spectra.

In this article, we report the first observation of gaseous UF_x^- ($x = 2-4$) anionic species and their characterization using photoelectron spectroscopy (PES) and quantum chemical calculations. Vibrationally resolved photoelectron spectra have been obtained for each species at several photon energies. The photoelectron spectra show all three species have much lower electron binding energies than the previously

a)Electronic mail: junli@tsinghua.edu.cn

b)Electronic mail: lai-sheng_wang@brown.edu

observed UF_5^- and UF_6^- .^{31,35} The adiabatic detachment energies (ADEs) of the anions or the electron affinities (EAs) of the corresponding neutral UF_x ($x = 2-4$) species are accurately measured. The geometries, bond order indexes, and ADEs of the UF_x^- ($x = 2-4$) species are calculated. The experimental spectra are qualitatively understood using the calculated electron configurations of UF_x^- ($x = 2-4$).

II. EXPERIMENTAL AND THEORETICAL METHODS

A. Photoelectron spectroscopy

The experiment was carried out using a magnetic-bottle PES apparatus equipped with a laser vaporization cluster source, details of which have been published in Ref. 50. In brief, a uranium plasma was generated by laser vaporization of a uranium disk target (Goodfellow Corporation) with a helium carrier gas containing a small amount of F_2 . Plasma reactions between the laser-vaporized uranium atoms and F_2 produced the desired UF_x^- ($x = 2-4$) species. The F_2 concentrations were adjusted to optimize a given UF_x^- species by mixing a 0.05% F_2 -in-helium gas with a 5% Ar-in-helium gas. Because of the high reactivity between U and F_2 , stable UF_2^- and UF_3^- anion beams were produced with the residual F_2 in the gas line after exposure to the F_2 gas, whereas little UF^- anion could be produced under our experimental conditions. The anions were entrained in the Ar/He carrier gas and underwent a supersonic expansion to form a cold and collimated molecular beam after passing a skimmer. Anions from the beam were extracted perpendicularly and analyzed by a time-of-flight mass spectrometer. The anions of interest were mass-selected and decelerated before being photodetached by a laser beam at 193 nm (6.424 eV) from an ArF excimer laser, and 266 nm (4.661 eV), 355 nm (3.496 eV), or 532 nm (2.331 eV) from a Nd-YAG laser. Photoelectrons were analyzed in a 3.5 m long flight tube and the photoelectron spectra were calibrated by the known spectra of Au^- and Bi^- . The resolution of the apparatus, $\Delta E_k/E_k$, was better than 2.5%, i.e., ~ 25 meV for 1 eV electrons.

B. Theoretical methods

Theoretical calculations were carried out for UF_x^- ($x = 1-6$) using spin-unrestricted Kohn-Sham density functional theory.⁵¹ The generalized-gradient approach with PBE exchange-correlation functional⁵² was used as implemented in the Amsterdam Density Functional program (ADF 2010.01).⁵³⁻⁵⁵ In these calculations, we used the PBE functional with zero-order-regular approximation (ZORA)⁵⁶ for the scalar relativistic (SR) and spin-orbit (SO) effects. The frozen core approximation was applied to the $[1s^2]$ core of F and the $[1s^2-5d^{10}]$ core of U, with the rest of the electrons explicitly treated variationally. The uncontracted Slater basis sets with triple- ζ plus two polarization functions (TZ2P) were used for the valence electrons.⁵⁷ The geometries were fully optimized for various possible electron configurations and vibrational frequencies were computed analytically. Mulliken population analysis,⁵⁸ Mayer bond order,⁵⁹ Gopinathan-Jug (G-J) bond orders,⁶⁰ and three-types of Nalewajski-Mrozek

(N-M) bond orders,⁶¹ were performed to understand the U-F bonding in the UF_x complexes. Because of the nearly degenerate spin multiplets, we also carried out geometry optimizations using the hybrid B3LYP functional⁶²⁻⁶⁴ and subsequent CCSD(T) single-point energy calculations with the NWChem program.⁶⁴ In these calculations, the aug-cc-pVTZ (AVTZ hereafter) basis set was used for F,⁶⁵ and SDD pseudopotential and basis set with 30 valence electrons were used for uranium,⁶⁶ where the scalar relativistic effects were included through the quasi-relativistic pseudopotential.

III. EXPERIMENTAL RESULTS

The photoelectron spectra of UF_x^- ($x = 2-4$) at four different photon energies are shown in Figs. 1-3, respectively. The observed PES bands are labeled with letters (X, A, B, ...) and the measured vertical detachment energies (VDEs), ADEs, and vibrational frequencies are summarized in Table I. The use of the Ar-seeded helium carrier gas was shown previously to produce very cold gold cluster anions.⁶⁷ Very recently high resolution photoelectron imaging experiments showed that with the Ar-seeded helium carrier gas we could produce vibrationally cold Au_4^- clusters, for which vibrational hot bands were completely eliminated.⁶⁸ The sharp onset in the 532 nm spectra of UF_2^- (Fig. 1(a)) and UF_3^- (Fig. 2(a)) suggested that these anions were vibrationally cold. We only observed very weak vibrational hot band in the 532 nm spectrum of UF_4^- (Fig. 3(a)). The cold anions and the vibrationally resolved photoelectron spectra at 532 nm were critical for us to evaluate the ADEs for the anions. In each spectrum, the X band represents the transition from the anionic ground electronic state to that of the neutral. The A, B, ... bands denote transitions from the anionic ground electronic state to the excited states of the neutrals. The weak broad features in the energy region from 2 to 4 eV in the UF_2^- spectra are labeled with low-case letters *a, b, c...* and their peak positions are also listed in Table I.

A. Photoelectron spectra of UF_2^-

The photoelectron spectrum of UF_2^- at 532 nm (Fig. 1(a)) shows a number of well-resolved features (X and A) in the low binding energy range and three weak peaks (B, C, D). The low binding energy features seem to consist of two vibrational progressions. The progression labeled as X has a VDE of 1.18 ± 0.03 eV with a vibrational spacing of 580 ± 30 cm^{-1} . Each vibrational peak has a splitting of about 20 meV, indicating excitation of another vibrational mode with a low frequency of about 160 ± 30 cm^{-1} . The ADE is defined by the 0-0 transition to be 1.16 ± 0.03 eV (Table I), which represents the EA of UF_2 . The progression labeled with A has an origin at 1.31 ± 0.03 eV with an average vibrational spacing of 510 ± 30 cm^{-1} . Each vibrational peak of band A is also fairly broad, indicating unresolved low frequency vibrational features. Three weak and relatively sharp features labeled as B, C, and D are observed at 1.76 ± 0.03 eV, 1.84 ± 0.03 eV, and 1.90 ± 0.03 eV, respectively.

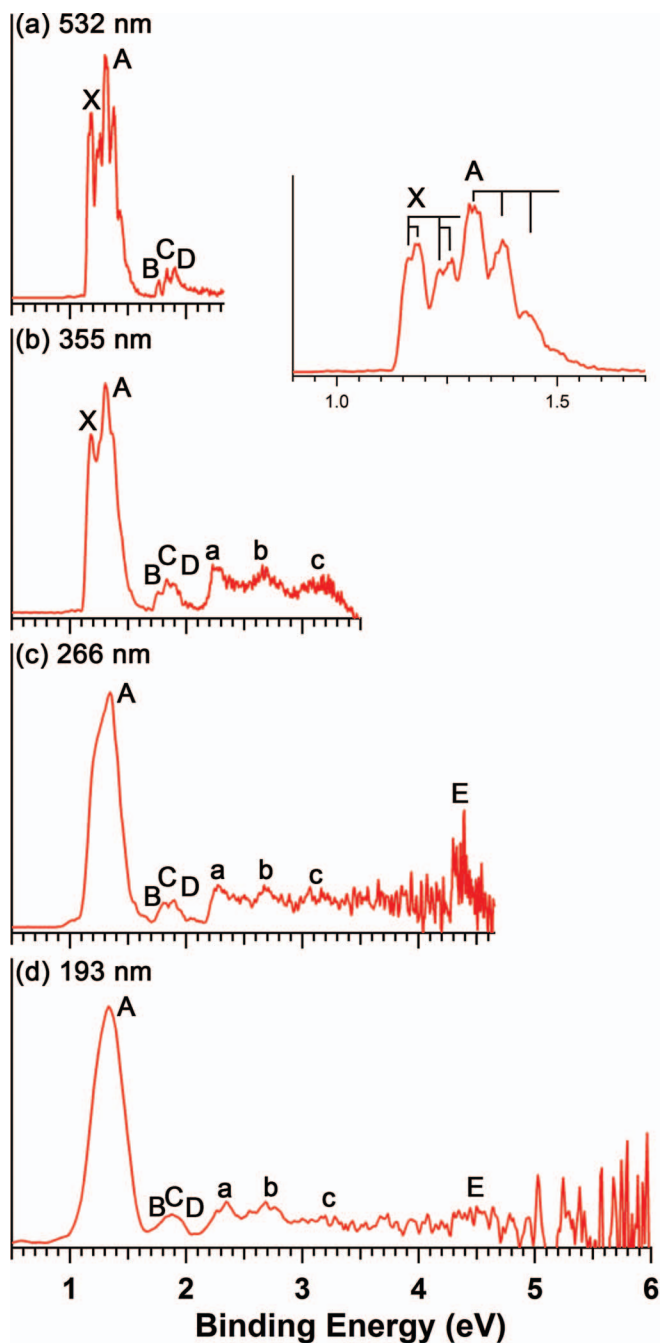


FIG. 1. Photoelectron spectra of UF_2^- at (a) 532 nm, (b) 355 nm, (c) 266 nm, and (d) 193 nm. The vertical lines in the inset indicate vibrational structures.

The spectra of UF_2^- at 355 nm (Fig. 1(b)) and 266 nm (Fig. 1(c)) show weak and almost continuous signals in the 2–4 eV region. Three broad features can be tentatively identified as *a* at ~ 2.2 eV, *b* at ~ 2.7 eV, and *c* at ~ 3.2 eV. Another feature E is observed at ~ 4.3 eV in the 266 nm spectrum (Fig. 1(c)), but it became rather weak in the 193 nm spectrum (Fig. 1(d)), most likely due to the severe noise in the high binding energy range that resulted in poor signal to noise ratios after background subtraction. The continuous signals observed between 2 and 4 eV indicate a high density of electronic states in this energy region in neutral UF_2 . They are similar to those observed in the photoelectron spectra of

UO_2^- observed recently, as a result of two-electron detachment transitions.⁴⁹

B. Photoelectron spectra of UF_3^-

The 532 nm spectrum of UF_3^- (Fig. 2(a)) displays three broad features, an intense band X and two relatively weak bands A and B. The intense band X with a VDE of 1.16 ± 0.03 eV contains congested vibrational features. The ADE of band X is evaluated by drawing a tangential line along the leading edge and then adding the instrumental resolution to the intersection with the binding energy axis. The so

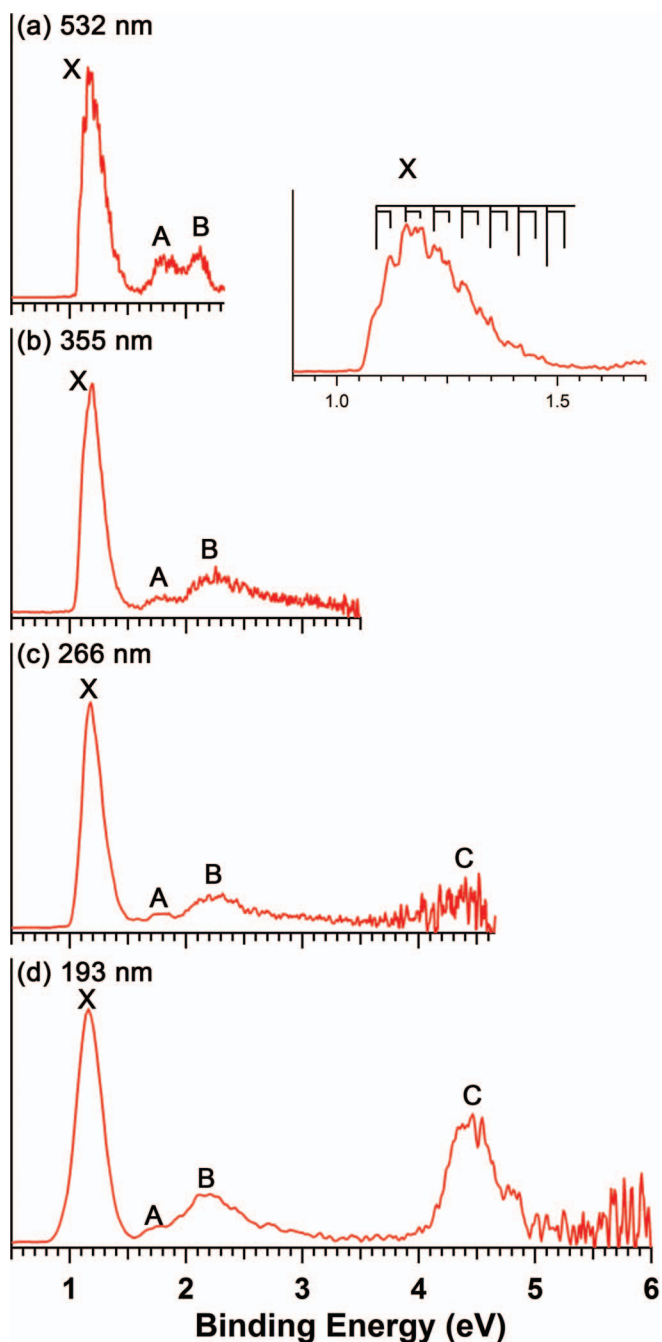


FIG. 2. Photoelectron spectra of UF_3^- at (a) 532 nm, (b) 355 nm, (c) 266 nm, and (d) 193 nm. The vertical lines in the inset indicate vibrational structures.

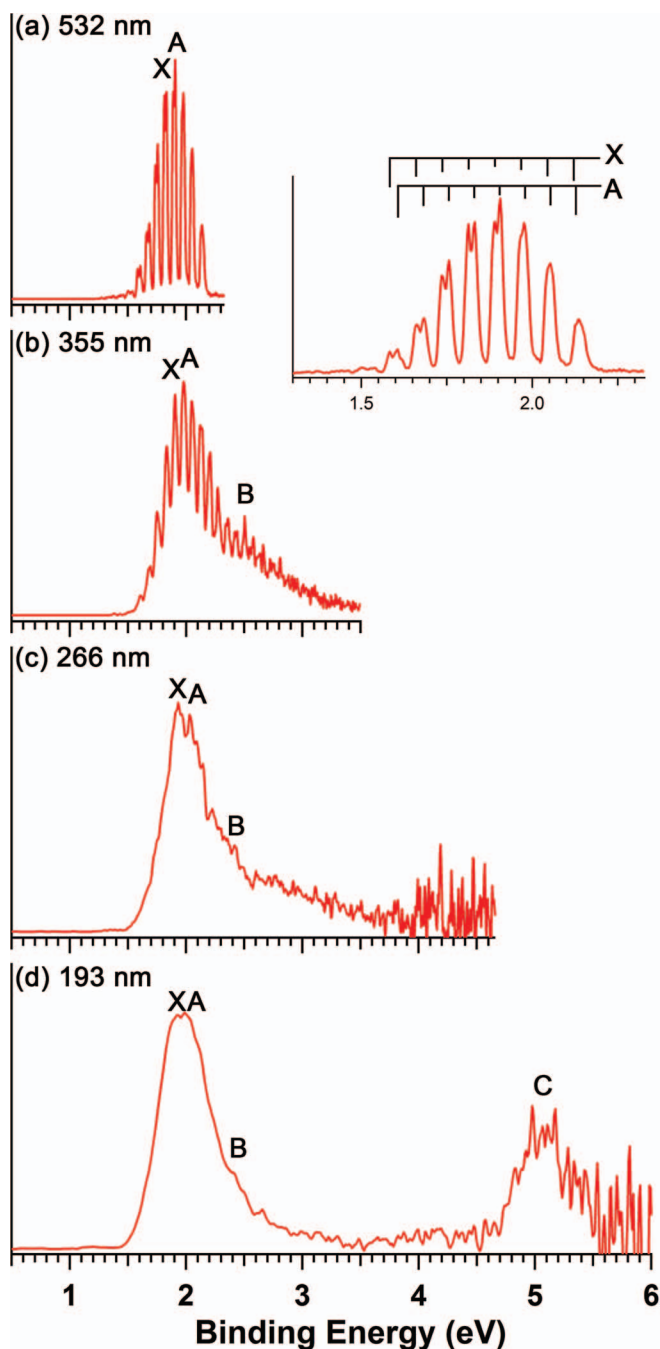


FIG. 3. Photoelectron spectra of UF_4^- at (a) 532 nm, (b) 355 nm, (c) 266 nm, and (d) 193 nm. The vertical lines in the inset indicate vibrational structures.

obtained ADE for UF_3^- is 1.09 ± 0.03 eV (Table I), which is also the EA of neutral UF_3 . Band X contains two possible vibrational progressions, a long progression with a spacing of 530 ± 50 cm^{-1} and tentatively a short progression with a spacing of 260 ± 50 cm^{-1} . The weak band A has an estimated VDE of ~ 1.8 eV. At 355 nm (Fig. 2(b)), band B is observed to be quite broad, which may be due to extensive vibrational excitations or multiple detachment transitions. The VDE of band B is estimated to be ~ 2.2 eV. Following a large energy gap, a broad band C is observed at a VDE of ~ 4.5 eV in the 266 and 193 nm spectra.

TABLE I. Observed vertical detachment energies (VDEs) and the first adiabatic detachment energy (ADE) for UF_x^- ($x = 2-4$) and the U–F stretching frequencies of the neutral ground state.^a

	Observed features	UF_2^-	UF_3^-	UF_4^-
VDEs (eV)	X	1.18(3)	1.16(3)	1.97(3)
	A	1.31(3)	~ 1.8	1.98(3)
	B	1.76(3)	~ 2.2	2.50(3)
	C	1.84(3)	~ 4.5	~ 5.1
	D	1.90(3)		
	E	~ 4.3		
	a	~ 2.2		
	b	~ 2.7		
	c	~ 3.2		
ADE (eV) ^b		1.16(3)	1.09(3)	1.58(3)
Frequency (cm^{-1})		580(30)	530(50)	620(20)

^aNumbers in parentheses represent the uncertainty in the last digits.

^bThis also represents the electron affinity of the neutral UF_x species.

C. Photoelectron spectra of UF_4^-

The 532 nm spectrum of UF_4^- shown in Fig. 3(a) displays a nice vibrational progression. Each vibrational peak seems to be a doublet. Careful examination shows that there are two similar vibrational progressions, which should correspond to two nearly degenerate detachment channels. The ground state vibrational progression X has a slightly higher frequency of 620 ± 20 cm^{-1} , whereas the slightly higher energy progression A has a frequency of 600 ± 20 cm^{-1} . The 0–0 transition of band X define an ADE of 1.58 ± 0.03 eV (Table I), which represents the EA of UF_4 . A very weak hot band was observed around 1.50 eV. The ADE of band A is measured to be 1.61 ± 0.03 eV. The VDEs of bands X and A cannot be measured from the 532 nm, because of the cut-off in the high binding side. The 355 nm spectrum (Fig. 3(b)) shows that the $v = 5$ vibrational level defines the VDEs for bands X and A, which are measured from the 532 nm as 1.97 ± 0.03 eV and 1.98 ± 0.03 eV, respectively. The 355 nm spectrum (Fig. 3(b)) reveals a new band B also with an extensive vibrational progression that overlaps with those of bands X and A. The VDE of band B is estimated to be 2.50 ± 0.03 eV. The 266 nm spectrum (Fig. 3(c)) does not reveal additional bands, while the 193 nm spectrum (Fig. 3(d)) shows a broad feature C at a VDE of ~ 5.1 eV following a large energy gap.

IV. THEORETICAL RESULTS

The symmetries, ground-state electron configurations, and structural parameters for UF_x and UF_x^- ($x = 1-6$) are summarized in Table II, where the calculated first ADEs for the anions are also given. The geometry optimizations were performed on UF_x^- ($x = 1-6$) with various electron configurations. The most stable configurations for UF_x^- ($x = 1-6$) anions are $\text{U}(5f)^3(7s)^2(6d)^1$, $\text{U}(5f)^3(7s)^2$, $\text{U}(5f)^3(7s)^1$, $(5f)^3$, $\text{U}(5f)^2$, and $\text{U}(5f)^1$, respectively. While these electron configurations and molecular symmetries are consistent with previous calculations on the neutral species,⁴⁴ they should be considered as tentative because of the complexity arising from the strong electron correlation and configuration-mixing due

TABLE II. Molecular symmetries, electron configurations, geometries, and energies of UF_x and UF_x^- ($x = 1 - 6$).^a

	Symmetry	Configuration	U-F bond length (\AA) ^b	$\angle\text{FUF}$ (deg) ^b	ADE ^{SO} (eV)
UF_6^-	O_h	$(5f)^1(7s)^0$	2.095	90.0	4.07
UF_5^-	C_{4v}	$(5f)^2(7s)^0$	2.128(<i>a</i>), 2.125(<i>e</i>)	102.6, 87.3	2.63
UF_4^-	D_{2d}	$(5f)^2(7s)^1$	2.147	106.5, 110.0	1.66
UF_3^-	C_{3v}	$(5f)^3(7s)^1$	2.136	110.0	0.89
UF_2^-	C_{2v}	$(5f)^3(7s)^2$	2.092	105.2	0.88
UF^-	$\text{C}_{\infty v}$	$(5f)^3(7s)^2(6d)^1$	2.075	...	0.25
UF_6	O_h	$(5f)^0(7s)^0$	2.021	90.0	
UF_5	C_{4v}	$(5f)^1(7s)^0$	2.032(<i>a</i>), 2.036(<i>e</i>)	95.89(<i>ae</i>), 89.4(<i>ee</i>)	
UF_4	D_{2d}	$(5f)^2(7s)^0$	2.067	109.2, 109.8	
UF_3	C_{3v}	$(5f)^3(7s)^0$	2.066	102.0	
UF_2	C_{2v}	$(5f)^3(7s)^1$	2.054	101.7	
UF	$\text{C}_{\infty v}$	$(5f)^3(7s)^2$	2.022	...	

^aAll the electron configurations, bond lengths, and bond angles are calculated using PBE functional with SO-ZORA Hamiltonian.

^b*a* and *e* denote axial and equatorial ligands, respectively.

to spin-orbit coupling. For instance, theoretical analyses with only SR effects cannot resolve the debate regarding the geometry of the UF_4 molecule because its $(t_2)^2$ electron configuration is in principle subject to a Jahn-Teller distortion. With spin-orbit coupling the t_2 MOs under T_d symmetry transform into $u_{3/2} + e_{5/2}$ spinors in double-group symmetry. Our preliminary SO-ZORA calculations with PBE functional show that the quadruply degenerate $u_{3/2}$ spinor is well below the $e_{5/2}$ spinor (by ~ 0.63 eV), implying a $(u_{3/2})^2$ ground state electron configuration, which is still Jahn-Teller active. Therefore, the geometry slightly distorts into D_{2d} symmetry even with spin-orbit coupling, but the distortion is nearly negligible relative to T_d symmetry because of the weak coupling between the $5f^x$ states, as shown in Table II. For UF_4^- , the most stable configuration at SR level is $5f^3$. However, with inclusion of SO effects, the most stable configuration is $5f^2 7s^1$. It is likely that the ground state of UF_4^- involves a strong mixing of the $5f^3$ and $5f^2 7s^1$ configurations.

V. DISCUSSION

Figure 4 depicts the contours of the occupied valence molecular orbitals of UF_x^- ($x = 2-4$) based on SR calculations. Quantitative assignments of the PES spectra of these open-shell species to specific electronic states of the neutrals are challenging because of the strong electron correlation and spin-orbit effects in the initial and final states involved in the electron detachment, as demonstrated in our recent detailed study of UO_2^- .⁴⁹ Here we propose qualitative assignments of the photoelectron spectra on the basis of the MO configurations and the drastically different detachment cross sections for the $5f$ or $7s$ -based MOs. Our previous PES studies on UF_5^- and UCl_5^- show that the detachment cross sections for the $5f$ -based MOs are much smaller relative to those of the ligand-based MOs.^{31,69}

A. UF_2^- and strong multi-electron transitions

The UF_2^- anion has an electron configurations of $\text{U}(5f)^3(7s)^2$ and neutral UF_2 has a $\text{U}(5f)^3(7s)^1$ configuration,

as shown in Table II and Fig. 4(a). Hence, the first detachment channel should correspond to removal of a $7s$ electron, resulting in both a quintet and triplet final state. At the SR level, the triplet neutral state is 0.075 eV higher than the quintet state. This energy difference is in good agreement with the experimental energy separation between the X and A bands in the photoelectron spectra of UF_2^- (~ 0.13 eV in Table I). Thus, the ground state of UF_2 should correspond to the quintet state and the A band should correspond to the triplet final state. The relatively high intensities of the X and A bands are consistent with the high electron detachment cross sections expected for a $7s$ -based MO. Electron detachments from the three unpaired $5f$ -based MOs should each produce a triplet final state with close energies and should correspond to the weak and relatively sharp features B, C, and D. The very weak intensities of these peaks relative to the X and A bands are consistent with electron detachment from $5f$ -based MOs. Electron detachment from the ligand-based F2p MOs should have high electron binding energies, corresponding to the relatively broad band E at ~ 4.3 eV. As will be seen below, the

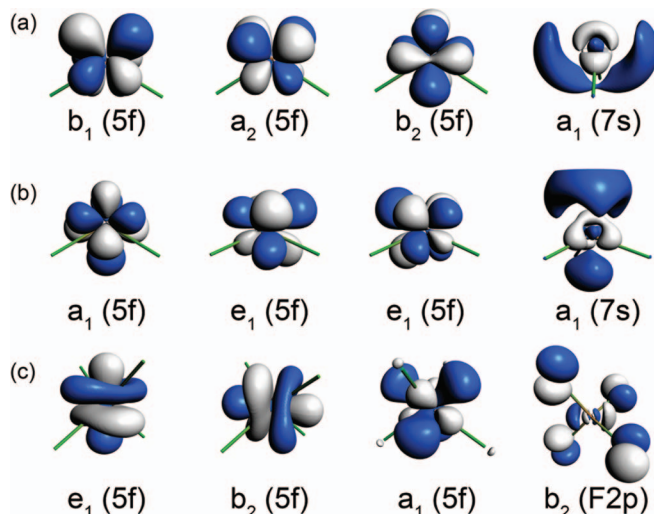


FIG. 4. Contours of the scalar-relativistic valence molecular orbitals of (a) UF_2^- (C_{2v}), (b) UF_3^- (C_{3v}), and (c) UF_4^- (D_{2d}).

binding energies for electron detachment from the F2p based MOs all have similarly high binding energies in the UF_3^- and UF_4^- cases as well.

Hence, no more one-electron detachment channels are expected between 2 and 4 eV. However, almost continuous transitions are observed in this photoelectron spectral region, as seen in Fig. 1 (bands labeled as *a*, *b*, *c*). These observations are reminiscent of the photoelectron spectra of the linear UO_2^- anion, which has a $\text{U}(7s^25f^1)$ electron configuration.⁴⁹ Because of the strong correlation between the pair of 7s electrons, an unprecedented number of two-electron transitions were observed as a result of detaching one 7s electron and simultaneous excitation of the other 7s electron to higher-lying unoccupied 7f orbitals. Such strong electron correlation effects between electrons in s-type orbitals have been commonly observed in photoionization of atoms with ns^2 configurations.⁷⁰ The nearly continuous PES features observed from 2 to 4 eV in the spectra of UF_2^- are most likely due to such multi-electron transitions, further confirming the $\text{U}(5f^3(7s)^2)$ electron configuration for UF_2^- .

Our calculated ADE for UF_2^- is 0.88 eV (Table II), in reasonable agreement with the experimental value of 1.16 eV. We have shown previously that DFT calculations tend to underestimate the electron binding energies for U-containing complexes.^{31,71–73} The U–F symmetric stretching frequency of the neutral UF_2 was calculated to be 554 cm^{-1} previously,⁴⁴ in good agreement with the measured frequency for the ground state band X (580 cm^{-1}). The U–F bond length decrease slightly (by 0.038 \AA) in UF_2 relative to the anion (Table II), consistent with the short U–F vibrational progression observed in the X band (Fig. 1(a)). The $\angle\text{FUF}$ angle in UF_2 is decreased by 3.5° , in agreement with the observed low-frequency vibrational excitation in the X band, which should be due to the bending mode.

B. UF_3^-

The UF_3^- anion has a quintet ground state with a $\text{U}(5f^3(7s)^1)$ electronic configuration while neutral UF_3 has a $\text{U}(5f^3(7s)^0)$ configuration (Table II and Fig. 4(b)). The first detachment channel is then from removal of the 7s-based a_1 electron (Fig. 4(b)), resulting in the ground state band X (Fig. 2). The strong relative intensity of this band is consistent with detachment from a 7s-based orbital. The next detachment channel should correspond to the removal of the 5f-based a_1 electron, corresponding to the weak band A. Detachment from the degenerate 5f-based e_1 orbital (Fig. 4(b)) should correspond to the broad band B. The broad width of band B is likely a result of the Jahn-Teller effect, expected from detachment from the degenerate e_1 orbital. The relative weak intensities of bands A and B are consistent with their 5f characters. The broad band C at 4.45 eV should come from detachment of F2p-based MOs. It is interesting to note that all the observed PES bands for UF_3^- correspond to one-electron detachment transitions. Unlike the UF_2^- case above, there is no evidence of multi-electron transitions. This observation provides indirect confirmation for the $\text{U}(5f^3(7s)^1)$ electron configuration of UF_3^- . We would expect strong multi-

electron transitions for a $\text{U}(5f)^2(7s)^2$ configuration because of the strong correlation effects of the 7s electrons, as observed for UF_2^- above and UO_2^- previously.⁴⁹

The ADE of UF_3^- is calculated to be 0.89 eV, again underestimated in comparison with the experimental value of 1.09 eV (Table I). Both the ground states of UF_3^- and UF_3 have C_{3v} symmetry, but the U–F bond length and $\angle\text{FUF}$ bond angle decrease significantly in the neutral (Table II), suggesting a long vibrational progression in the symmetric vibrational mode and also major Franck-Condon activities in the umbrella mode. These structural changes are in agreement with the broad and congested PES band observed for the ground state transition (Fig. 2(a)). The frequency of the totally symmetric U–F breathing mode of UF_3 was calculated to be 543 cm^{-1} previously,⁴⁴ in good agreement with the main vibrational progression of 530 cm^{-1} . The extensive Franck-Condon activities in both the stretching and bending modes of UF_3 would be expected to produce a very complicated and congested ground state vibrational progression, as observed experimentally.

C. UF_4^-

The ground state electron configuration of the UF_4^- anion is more complicated. At the SR level, it has a $5f^3$ configuration in its ground state. However, when SO coupling is included, the configuration becomes $5f^27s^1$. It is possible that the ground state of UF_4^- is multi-configurational with strong mixing of the two configurations. The relatively strong intensities of all the three observed PES bands at low binding energies are consistent with strong contributions of 7s characters in each of the detachment channel. The broad band C at $\sim 5.1\text{ eV}$ should come from detachment of F2p-based orbitals. There is a slight increase of the binding energies of this detachment feature from UF_2^- to UF_4^- (Figs. 1–3). The ADE of UF_4^- is calculated to be 1.66 eV, in good agreement with the measured value of 1.58 eV (Table I). There is a large U–F bond length reduction in the neutral UF_4 ground state (by 0.08 \AA) and little change in the $\angle\text{FUF}$ bond angles, in excellent agreement with the long vibrational progression (Fig. 3(a)), which should be due to the totally symmetric stretching mode with no discernible activity of any bending modes. The previously calculated frequency for the U–F breathing mode was 598 cm^{-1} ,⁴⁴ close to the experimentally measured frequency of 620 cm^{-1} . Our experiment indicates that the first excited state of UF_4 (band A) is nearly degenerate with the ground state (band X) and they have similar structures. In fact, the observation of a simple stretching vibrational progression for the ground state detachment transition without any hint of bending excitation suggests that both UF_4^- and UF_4 in their ground states may possess the high symmetry T_d structure, even though our current DFT calculations suggest a very slight distortion to a D_{2d} structure for both the anion and neutral uranium tetra-fluoride.

The low oxidation-state UF_x^- species with open 5f and 7s shells are challenging electronic systems. Advanced *ab initio* wavefunction calculations with both dynamic and static electron correlations and relativistic effects (including

TABLE III. The calculated Mulliken charges and bond orders of UF_x^- ($x = 1-6$) based on different bonding index schemes.

	Charge		Bond order				
	Q(U)	Q(F)	Mayer	G-J	N-M(1)	N-M(2)	N-M(3)
UF_6^-	2.32	-0.55	0.64	1.02	1.36	1.64	1.41
UF_5^-	1.90	-0.57	0.56, 0.62	0.88, 0.93	1.34, 1.39	1.67, 1.69	1.35, 1.39
UF_4^-	1.19	-0.55	0.53	0.90	1.50	1.72	1.50
UF_3^-	0.51	-0.50	0.43	0.93	1.63	1.74	1.58
UF_2^-	-0.25	-0.38	0.30	1.09	1.90	1.81	1.79
UF^-	-0.62	-0.38	0.36	1.20	2.78	2.28	2.23

spin-orbit coupling) are necessary to provide quantitative interpretations of the PES data. The rich electronic structure information would be ideal for verifying new computational methods for accurate treatments of the electronic structures of open-shell actinide compounds.

D. Trend of chemical bonding in UF_x^- ($x = 1-6$)

The calculated Mulliken charges and bond orders of UF_x^- ($x = 1-6$) from different bond index schemes are summarized in Table III. The electron density on the U atom decreases steadily from UF^- to UF_6^- , with the net charge increment of 0.37 |e|, 0.76 |e|, 0.68 |e|, 0.71 |e|, and 0.42 |e| with each additional F coordination from UF^- to UF_6^- . These results suggest that the U-F bonds are highly ionic in UF_5^- and UF_6^- with U at higher oxidation states. We observed similarly strong ionic bonding in UCl_5^- in a recent study.⁶⁷ Except for the Mayer bond orders, the G-J and all N-M bond orders suggest that the U-F bond becomes weaker from UF^- to UF_6^- . This trend is consistent with the bond dissociation energies calculated for UF_x ($x = 1-6$).^{45,74}

The U-F bond length increases from UF^- to UF_4^- and decreases from UF_4^- to UF_6^- . The UF_5^- and UF_6^- molecules have larger electrostatic interactions between the U and F atoms due to the large positive charge on U (Table III). The calculated ADEs based on the SO-ZORA approach with the PBE functional are systematically underestimated in comparison to the experimental values, consistent with our previous finding that DFT with approximate GGA exchange-correlation functionals fail to predict accurate electron detachment energies.^{31,71-73} However, the trend of the calculated ADEs is consistent with the experimental observations: when the oxidation state of the U increases from 0 in UF^- to V in UF_6^- , the ADE increases significantly. The higher EA with increasing F coordination is derived from the increased positive charge on the U center in neutral UF_x .

VI. CONCLUSIONS

The low oxidation-state UF_x^- ($x = 2-4$) species are observed and investigated using photoelectron spectroscopy and theoretical calculations. Vibrationally resolved photoelectron spectra are reported for all three species and the electron affinities of the three neutral UF_x ($x = 2-4$) species are accurately measured. The observed spectral features are qual-

itatively understood on the basis of the calculated electron configurations and the large differences of detachment cross sections from 5f or 7s-based orbitals. The electron binding energies of F2p-based orbitals are quite high and increases steadily from $x = 2-4$. Strong multi-electron transitions are observed for UF_2^- , due to its $5f^37s^2$ configuration. As the F coordination increases in UF_x^- , the U-F bond lengths increase and the bond strengths decrease, consistent with the calculated bond orders. The low oxidation-state UF_x^- species possess rich electronic structures and are ideal test cases to verify computational methods for accurate treatment of actinide compounds.

ACKNOWLEDGMENTS

This work was supported by the U.S. Department of Energy, Office of Basic Energy Sciences under Grant No. DE-FG02-11ER16261 (W.L.L., T.J., G.V.L., and L.S.W.). The theoretical work was supported by NSFC (20933003, 91026003, 21201106) of China (H.S.H., J.S., and J.L.). The calculations were performed using the Tsinghua National Laboratory for Information Science and Technology. A portion of the calculations was performed using EMSL, a national scientific user facility sponsored by the US Department of Energy's Office of Biological and Environmental Research and located at the Pacific Northwest National Laboratory, USA.

¹L. R. Morss, N. M. Edelstein, and J. Fuger, *The Chemistry of the Actinide and Transactinide Elements* (Springer, Dordrecht, Netherlands, 2006), Vol. 1.

²M. Kimura, V. Schomake, and D. W. Smith, *J. Chem. Phys.* **48**, 4001 (1968).

³J. H. Levy, J. C. Taylor, and P. W. Wilson, *J. Chem. Soc. Dalton Trans.* **1976**, 219.

⁴R. S. McDowell, L. B. Aspree, and R. T. Paine, *J. Chem. Phys.* **61**, 3571 (1974).

⁵R. T. Paine, R. S. McDowell, L. B. Aspree, and L. H. Jones, *J. Chem. Phys.* **64**, 3081 (1976).

⁶L. H. Jones, B. I. Swanson, and S. A. Ekberg, *J. Phys. Chem.* **88**, 1285 (1984).

⁷K. R. Kunze, R. H. Hauge, D. Hamill, and J. L. Margrave, *J. Chem. Phys.* **65**, 2026 (1976).

⁸K. R. Kunze, R. H. Hauge, D. Hamill, and J. L. Margrave, *J. Phys. Chem.* **81**, 1664 (1977).

⁹W. B. Lewis, L. B. Aspree, L. H. Jones, R. S. McDowell, S. W. Rabideau, A. H. Zeltmann, and R. T. Paine, *J. Chem. Phys.* **65**, 2707 (1976).

¹⁰R. McDiarmid, *J. Chem. Phys.* **65**, 168 (1976).

¹¹E. R. Bernstein and G. R. Meredith, *Chem. Phys.* **24**, 289 (1977).

¹²Y. M. Bosworth, R. J. H. Clark, and D. M. Rippon, *J. Mol. Spectrosc.* **46**, 240 (1973).

¹³J. C. Miller, S. W. Allison, and L. Andrews, *J. Chem. Phys.* **70**, 3524 (1979).

¹⁴R. Rianda, R. P. Frueholz, and A. Kuppermann, *J. Chem. Phys.* **70**, 1056 (1979).

¹⁵D. C. Cartwright, S. Trajmar, A. Chutjian, and S. Srivastava, *J. Chem. Phys.* **79**, 5483 (1983).

¹⁶N. Martensson, P. A. Malmquist, S. Svensson, and B. Johansson, *J. Chem. Phys.* **80**, 5458 (1984).

¹⁷P. J. Hay and R. L. Martin, *J. Chem. Phys.* **109**, 3875 (1998).

¹⁸J. Onoe, R. Sekine, K. Takeuchi, H. Nakamatsu, T. Mukoyama, and H. Adachi, *Chem. Phys. Lett.* **217**, 61 (1994).

¹⁹J. Onoe, K. Takeuchi, H. Nakamatsu, T. Mukoyama, R. Sekine, B. I. Kim, and H. Adachi, *J. Chem. Phys.* **99**, 6810 (1993).

²⁰S. Larsson and P. Pykko, *Chem. Phys.* **101**, 355 (1986).

- ²¹P. J. Hay, W. R. Wadt, L. R. Kahn, R. C. Raffenet, and D. H. Phillips, *J. Chem. Phys.* **71**, 1767 (1979).
- ²²D. A. Case and C. Y. Yang, *J. Chem. Phys.* **72**, 3443 (1980).
- ²³S. Larsson, J. S. Tse, J. L. Esquivel, and A. T. Kai, *Chem. Phys.* **89**, 43 (1984).
- ²⁴L. Gagliardi, A. Willetts, C. K. Skylaris, N. C. Handy, S. Spencer, A. G. Ioannou, and A. M. Simper, *J. Am. Chem. Soc.* **120**, 11727 (1998).
- ²⁵G. Schreckenbach, P. J. Hay, and R. L. Martin, *J. Comput. Chem.* **20**, 70 (1999).
- ²⁶Y. K. Han and K. Hirao, *J. Chem. Phys.* **113**, 7345 (2000).
- ²⁷E. R. Batista, R. L. Martin, P. J. Hay, J. E. Peralta, and G. E. Scuseria, *J. Chem. Phys.* **121**, 2144 (2004).
- ²⁸G. A. Shamov, G. Schreckenbach, and T. N. Vo, *Chem. Eur. J.* **13**, 4932 (2007).
- ²⁹A. Perez-Villa, J. David, P. Fuentealba, and A. Restrepo, *Chem. Phys. Lett.* **507**, 57 (2011).
- ³⁰F. Wei, G. S. Wu, W. H. E. Schwarz, and J. Li, *J. Chem. Theory Comput.* **7**, 3223 (2011).
- ³¹P. D. Dau, J. Su, H. T. Liu, D. L. Huang, F. Wei, J. Li, and L. S. Wang, *J. Chem. Phys.* **136**, 194304 (2012).
- ³²G. P. Jackson, J. K. Gibson, and D. C. Duckworth, *J. Phys. Chem. A* **108**, 1042 (2004).
- ³³R. D. Hunt, C. Thompson, P. Hassanzadeh, and L. Andrews, *Inorg. Chem.* **33**, 388 (1994).
- ³⁴K. R. Kunze, R. H. Hauge, and J. L. Margrave, *Inorg. Nucl. Chem. Lett.* **15**, 65 (1979).
- ³⁵P. D. Dau, H. T. Liu, D. L. Huang, and L. S. Wang, *J. Chem. Phys.* **137**, 116101 (2012).
- ³⁶G. V. Girichev, V. M. Petrov, N. I. Giricheva, E. Z. Zazorin, K. S. Krasnov, and Y. M. Kiselev, *J. Struct. Chem.* **24**, 61 (1983).
- ³⁷R. J. M. Konings, A. S. Booi, A. Kovacs, G. V. Girichev, N. I. Giricheva, and O. G. Krasnova, *J. Mol. Struct.* **378**, 121 (1996).
- ³⁸D. L. Hildenbrand, *J. Chem. Phys.* **66**, 4788 (1977).
- ³⁹D. L. Hildenbrand, *Pure Appl. Chem.* **60**, 303 (1988).
- ⁴⁰D. L. Hildenbrand, K. H. Lau, and R. D. Brittain, *J. Chem. Phys.* **94**, 8270 (1991).
- ⁴¹V. N. Bukhmarina, Y. B. Predtechensky, and L. D. Shcherba, *J. Mol. Struct.* **218**, 33 (1990).
- ⁴²R. J. M. Konings and D. L. Hildenbrand, *J. Alloys Compd.* **271–273**, 583 (1998).
- ⁴³I. O. Antonov and M. C. Heaven, *J. Phys. Chem. A* **117**, 9684 (2013).
- ⁴⁴E. R. Batista, R. L. Martin, and P. J. Hay, *J. Chem. Phys.* **121**, 11104 (2004).
- ⁴⁵J. E. Peralta, E. R. Batista, G. E. Scuseria, and R. L. Martin, *J. Chem. Theory Comput.* **1**, 612 (2005).
- ⁴⁶D. A. Pantazis and F. Neese, *J. Chem. Theory Comput.* **7**, 677 (2011).
- ⁴⁷L. Joubert and P. Maldivi, *J. Phys. Chem. A* **105**(39), 9068 (2001).
- ⁴⁸A. V. Zaitsevskii, *Radiochemistry* **55**, 353 (2013).
- ⁴⁹W. L. Li, J. Su, T. Jian, G. V. Lopez, H. S. Hu, G. J. Cao, J. Li, and L. S. Wang, "Strong Electron Correlation in UO_2^{-f0} : A Photoelectron Spectroscopy and Relativistic Quantum Chemistry Study," *J. Chem. Phys.* (submitted).
- ⁵⁰L. S. Wang, H. S. Cheng, and J. W. Fan, *J. Chem. Phys.* **102**, 9480 (1995).
- ⁵¹P. Hohenberg and W. Kohn, *Phys. Rev.* **136**, B864 (1964).
- ⁵²J. P. Perdew, K. Burke, and M. Ernzerhof, *Phys. Rev. Lett.* **77**, 3865 (1996).
- ⁵³ADF2010.01 Program, SCM, Theoretical Chemistry, Vrije Universiteit, Amsterdam, The Netherlands, 2009, see <http://www.scm.com>.
- ⁵⁴G. te Velde, F. M. Bickelhaupt, E. J. Baerends, C. F. Guerra, S. J. A. Van Gisbergen, J. G. Snijders, and T. Ziegler, *J. Comput. Chem.* **22**, 931 (2001).
- ⁵⁵C. F. Guerra, J. G. Snijders, G. te Velde, and E. J. Baerends, *Theor. Chem. Acc.* **99**, 391 (1998).
- ⁵⁶E. van Lenthe, E. J. Baerends, and J. G. Snijders, *J. Chem. Phys.* **99**, 4597 (1993).
- ⁵⁷E. Van Lenthe and E. J. Baerends, *J. Comput. Chem.* **24**, 1142 (2003).
- ⁵⁸R. S. Mulliken, *J. Chem. Phys.* **23**, 1833 (1955).
- ⁵⁹I. Mayer, *Chem. Phys. Lett.* **97**, 270 (1983).
- ⁶⁰M. S. Gopinathan and K. Jug, *Theor. Chim. Acta* **63**, 497 (1983).
- ⁶¹A. Michalak, R. L. DeKock, and T. Ziegler, *J. Phys. Chem. A* **112**, 7256 (2008).
- ⁶²A. D. Becke, *J. Chem. Phys.* **98**, 5648 (1993).
- ⁶³A. D. Becke, *Phys. Rev. A* **38**, 3098 (1988).
- ⁶⁴M. Valiev, E. J. Bylaska, N. Govind, K. Kowalski, T. P. Straatsma, H. J. J. Van Dam, D. Wang, J. Nieplocha, E. Apra, T. L. Windus, and W. de Jong, *Comput. Phys. Commun.* **181**, 1477 (2010).
- ⁶⁵Pc. Harihara and J. A. Pople, *Theor. Chim. Acta* **28**, 213 (1973).
- ⁶⁶W. Kuchle, M. Dolg, H. Stoll, and H. Preuss, *J. Chem. Phys.* **100**, 7535 (1994).
- ⁶⁷W. Huang and L. S. Wang, *Phys. Rev. Lett.* **102**, 153401 (2009).
- ⁶⁸Z. Yang, I. Leon, and L. S. Wang, *J. Chem. Phys.* **139**, 021106 (2013).
- ⁶⁹J. Su, P. D. Dau, C. F. Xu, D. L. Huang, H. T. Liu, F. Wei, L. S. Wang, and J. Li, *Chem. Asian J.* **8**, 2489 (2013).
- ⁷⁰S. Suzer, S. T. Lee, and D. A. Shirley, *Phys. Rev. A* **13**, 1842 (1976).
- ⁷¹P. D. Dau, J. Su, H. T. Liu, J. B. Liu, D. L. Huang, J. Li, and L. S. Wang, *Chem. Sci.* **3**, 1137 (2012).
- ⁷²P. D. Dau, J. Su, H. T. Liu, D. L. Huang, J. Li, and L. S. Wang, *J. Chem. Phys.* **137**, 064315 (2012).
- ⁷³J. Su, P. D. Dau, Y. H. Qiu, H. T. Liu, C. F. Xu, D. L. Huang, L. S. Wang, and J. Li, *Inorg. Chem.* **52**, 6617 (2013).
- ⁷⁴D. L. Hildenbrand and K. H. Lau, *J. Chem. Phys.* **94**, 1420 (1991).